Hindawi Publishing Corporation
The Scientific World Journal
Volume 2013, Article ID 612712, 6 pages
http://dx.doi.org/10.1155/2013/612712

Research Article

Kinetic Study on the Cs_XH_{3-X} $PW_{12}O_{40}$/Fe-SiO_2 Nanocatalyst for Biodiesel Production

Mostafa Feyzi,[1,2] Leila Norouzi,[1] and Hamid Reza Rafiee[1]

[1] *Faculty of Chemistry, Razi University, P.O. Box 6714967346, Kermanshah, Iran*
[2] *Nanoscience & Nanotechnology Research Center (NNRC), Razi University, P.O. Box 6714967346, Kermanshah, Iran*

Correspondence should be addressed to Mostafa Feyzi; dalahoo2011@yahoo.com

Received 2 September 2013; Accepted 20 October 2013

Academic Editors: H. Choi and D. Fu

Copyright © 2013 Mostafa Feyzi et al. This is an open access article distributed under the Creative Commons Attribution License, which permits unrestricted use, distribution, and reproduction in any medium, provided the original work is properly cited.

The kinetic of the transesterification reaction over the $Cs_XH_{3-X}PW_{12}O_{40}$/Fe-SiO_2 catalyst prepared using sol-gel and impregnation procedures was investigated in different operational conditions. Experimental conditions were varied as follows: reaction temperature 323–333 K, methanol/oil molar ratio = 12/1, and the reaction time 0–240 min. The $H_3PW_{12}O_{40}$ heteropolyacid has recently attracted significant attention due to its potential for application in the production of biodiesel, in either homogeneous or heterogeneous catalytic conditions. Although fatty acids esterification reaction has been known for some time, data is still scarce regarding kinetic and thermodynamic parameters, especially when catalyzed by nonconventional compounds such as $H_3PW_{12}O_{40}$. Herein, a kinetic study utilizing Gc-Mas in situ allows for evaluating the effects of operation conditions on reaction rate and determining the activation energy along with thermodynamic constants including ΔG, ΔS, and ΔH. It indicated that the $Cs_XH_{3-X}PW_{12}O_{40}$/Fe-SiO_2 magnetic nanocatalyst can be easily recycled with a little loss by magnetic field and can maintain higher catalytic activity and higher recovery even after being used 5 times. Characterization of catalyst was carried out by using scanning electron microscopy (SEM), X-ray diffraction (XRD), Fourier transform-infrared spectroscopy (FT-IR), N_2 adsorption-desorption measurements methods, thermal gravimetric analysis (TGA), and differential scanning calorimetry (DSC).

1. Introduction

Biodiesel is a fuel composed of monoalkyl esters of long chain fatty acids derived from renewable sources, such as vegetable oils and animal fats [1]. Due to oxygen content, biodiesel is a clean, nontoxic, and biodegradable fuel with low exhaust emissions, without the sulphur and carcinogen content [2]. Biodiesel is prepared via reaction between triglycerides and alcohol in the presence of a catalyst [3]. Transesterification reaction of oil and alcohol with homogeneous catalyst is the most common method for the preparation of biodiesel [4, 5]. However, the homogeneous catalyst has many drawbacks, such as the difficulty in product separation, and equipment corrosion requirement of large quantity of water, environmental pollution [6]. The use of heterogeneous catalysts to replace homogeneous ones is easily regenerated and has a less corrosive nature, leading to safer, cheaper, and more environment-friendly operations, [7]. Currently, the research is focused on sustainable solid acid catalysts for transesterification reaction. In addition, it is believed that solid acid catalysts have the strong potential than liquid acid catalyst [8]. HPW catalyst is a strong Brønsted acid, with high thermal stability and high solubility in polar solvents, and it has shown to be more active in FFA esterification reactions than mineral acid catalysts [8–12]. However, heteropolyacids have low surface areas and high solubility in polar solvents. These features make some difficulties in catalyst recovery and catalyst lifetime [13]. Therefore, salts of HPAs with large single valence ions, such as Cs^+, NH_4^+, and Ag^+, have attracted much fondness because these salts will increase in surface area and profound changes in solubility over the parent heteropolyacid [14, 15]. HPW can be supported on several kinds of support such as SiO_2, Al, ZrO_2, activated carbon, SiO_2-Al, and MCM-41 that SiO_2 is cheap, easily available, and easily surface modifiable [16–18].

In the present kinetic study, pseudo-first-order model was applied to correlate the experimental kinetic data of catalytic performance of the $Cs_XH_{3-X}PW_{12}O_{40}$/Fe-SiO_2 for

sunflower oil transesterification with methanol and the main thermodynamic parameters such as the effects of temperature on reaction rate, activation energy, entropy variation (ΔS), and enthalpy variation (ΔH) were determined; moreover, the effects of temperature on reaction rate and the order of reaction were assessed. Characterization of catalyst was carried out by using scanning electron SEM, XRD, FT-IR, N_2 adsorption-desorption measurements methods, TGA, and DSC methods.

2. Experimental

2.1. Fe-SiO_2 Support Preparation. All materials with analytical purity were purchased from Merck and used without further purification. Ferric nitrate ($Fe(NO_3)_3{\cdot}9H_2O$) and tetraethyl orthosilicate (TEOS) were selected as the source of ferric and silica, respectively. A typical procedure for the preparation of ferric-silica mixed oxide containing 60 wt% ferric was followed. Firstly, 30 mL TEOS was mixed with certain amount anhydrous ethyl alcohol (C_2H_5OH). Secondly, 35.234 gr $Fe(NO_3)_3{\cdot}9H_2O$ was dissolved with certain amount of anhydrous ethyl alcohol under stirring; also 30 gr of oxalic acid was dissolved in certain amount of anhydrous alcohol under stirring. In the final step, Fe and Si sols and oxalic acid were added simultaneously into the beaker under constant stirring to obtain a gel form. After the end of the above operations, the samples were aged for 90 min at 50°C. The obtained gel was dried in an oven (120°C, 12 h) to give a material denoted as the catalyst precursor. Finally, the catalyst precursor was calcined at 600°C for 6 h to produce magnetic solid catalyst. The Fe-SiO_2 supported 12-tungstophosphoric acid catalyst with 4 wt.% of aqueous solution HPW (based on the Fe-SiO_2 weight) were prepared by incipient wetness impregnation. The impregnated precursor was dried at 120°C for overnight and calcined at 600°C for 6 h.

Finally, the promoted catalyst by Cs was synthesized with $Cs/H_3PW_{12}O_{40}$ = 2 wt.%. The salt obtained by this procedure will be designated hereinafter as $Cs_XH_{3-X}PW_{12}O_{40}$/Fe-SiO_2, where X is the amount of protons per $[PW_{12}O_{40}]^{3-}$ anion in the salt.

2.2. Characterization of Catalyst

2.2.1. N_2 Physisorption Measurements. The specific surface area, total pore volume, and the mean pore diameter were measured using a N_2 adsorption-desorption isotherm at liquid nitrogen temperature (−196°C), using a NOVA 2200 instrument (Quantachrome, USA). Prior to the adsorption-desorption measurements, all the samples were degassed at 110°C in a N_2 flow for 2 h to remove the moisture and other adsorbates.

2.2.2. Scanning Electron Microscopy (SEM). The morphology of catalyst and precursor was observed by means of an S-360 Oxford Eng scanning electron microscopy.

2.2.3. Fourier Transform-Infrared Spectroscopy (FT-IR). Fourier transform infrared (FT-IR) spectra of the samples were obtained using a Bruker Vector 22 spectrometer in the region of 400–4000 cm^{-1}.

2.2.4. X-Ray Diffraction (XRD). X-ray diffraction (XRD) patterns of the catalysts were recorded on a diffractometer using CuK_α radiation. The intensity data were collected over a 2θ range of 15–75.

2.2.5. Thermal Gravimetric Analysis (TGA) and Differential Scanning Calorimetry (DSC). The TGA and DSC were carried out using simultaneous thermal analyzer (PerkinElmer) under a flow of dry air with a flow rate of 50 mL min^{-1}. The temperature was raised from 20 to 700°C using a linear programmer at a heating rate of 3°C min^{-1}.

2.3. Catalytic Tests. The type and quantity of methyl esters in the biodiesel samples were determined using gas chromatography-mass spectrometry (GC Agilent 6890N model and Mass Agilent 5973N model) equipped with a flame ionized detector (FID). A capillary column (HP-5) with column length (60 m), inner diameter (0.25 mm), and 0.25 μm film thickness was used with helium as the carrier gas. The temperature program for the biodiesel samples started at 50°C and ramped to 150°C at 10°C min^{-1}. The temperature was held at 150°C for 15 min and ramped to 280°C at 5°C min^{-1}. The holding time at the final temperature (250°C) was 5 min. Also, the injector was used from kind split/splitless.

2.4. Kinetic Studies. The transesterification of sunflower oil was carried out in a round bottomed flask fitted with a condenser and magnetic stirring system. The reaction system was heated to selected temperature in 50, 55, and 60°C. When the oil reached selected temperature, methanol/oil molar ratio = 12/1 and the catalyst amount (3 wt% related to oil weight) were added with continuous stirring (500 rpm). After completion of the reaction time (0–240 min), the sample concentration is calculated according to mole fraction at any time. The results can be seen in Table 1.

3. Kinetic Model

The mole fraction for the transesterification reaction was established. For the reaction stoichiometry requires 3 Mol of methanol (M) and 1 mol of triglyceride (TG) to give 3 mol of methyl ester (ME) and 1 Mol of glycerol (GL). Transesterification reaction comprises three consecutive reversible reactions, where 1 mol of ME is produced in each step and monoglycerides (MG) and diglycerides (DG) are intermediate products [19]. The kinetic model used in this work is based on the following assumptions.

(1) Firstly, k_{eq} should be considered not to depend on methanol concentration (due to its excess) (the reaction is considered pseudo-first order [20, 21]).

(2) Production of intermediate species is negligible (the result reaction is a one step).

(3) The chemical reaction occurred in the oil phase.

Table 1: Concentration of methyl ester (based on mole fraction) at temperatures of 60 (A), 55 (B), and 50°C (C), respectively.

Reaction time (s)	X_{ME}			$-\ln(1 - X_{ME})$		
	A	B	C	A	B	C
0	0.00	0.00	0.00	0.000000	0.000000	0.000000
30	0.32	0.24	0.14	0.385660	0.274437	0.150823
60	0.40	0.28	0.15	0.510826	0.328504	0.162519
90	0.42	0.34	0.24	0.590000	0.415515	0.274437
120	0.5819	0.43	0.30	0.872035	0.562119	0.356675
150	0.63	0.51	0.34	0.994252	0.713350	0.415515
180	0.70	0.57	0.38	1.203973	0.843970	0.478036
210	0.75	0.63	0.45	1.386294	0.994252	0.597837
240	0.81	0.65	0.50	1.660731	1.049822	0.693147

X_{ME}: concentration of methyl ester.
$-\ln(1 - X_{ME})$: triglyceride concentration.

Based on assumption (1),

$$-r = \frac{-d[TG]}{dt} = k[TG][\mathrm{ROH}]^3. \quad (1)$$

And based on assumption (2),

$$k' = k[\mathrm{ROH}]^3$$

$$-r = \frac{-d[TG]}{dt} = k'[TG] \quad (2)$$

$$\Longrightarrow \ln TG_0 - \ln TG = k' \cdot t.$$

According to the mass balance,

$$X_{ME} = 1 - \frac{[TG]}{[TG_0]}$$

$$[TG] = [TG_0][1 - X_{ME}] \quad (3)$$

$$\frac{dX_{ME}}{dt} = k'[1 - X_{ME}] \Longrightarrow -\ln(1 - X_{ME}) = k' \cdot t.$$

Based on this model and the experimental data, at first we calculated the concentration of methyl ester at different times (based on the moles fraction). Second, the rate constants at each temperature were obtained. Third, the preexponential factors and activation energies are obtained by plotting the logarithm of the rate constants (k) versus $1/T$ of absolute temperature using the Arrhenius equation and in the final stage thermodynamic parameters were obtained such as ΔS and ΔH.

4. Results and Discussion

4.1. Characterization of the Catalyst. The FT-IR spectra of $H_3PW_{12}O_{40}$, $Cs_XPW_{12}O_{40}$ and $Cs_XH_{3-X}PW_{12}O_{40}$/Fe-SiO_2 are shown in Figure 1. The Keggin anion of HPW consists of a central phosphorous atom tetrahedrally coordinated by four oxygen atoms and surrounded by twelve octahedral WO_6 units that share edges and corners in the structure.bands related to a Keggin structure (i(O–P–O) = 550 cm^{-1}, indicative of the bending of the central oxygen of P–O–P; νas(W–Oe–W) at 798 cm^{-1}, related to asymmetric stretching of tungsten with edge oxygen in W–O–W; νas(W–OcW) = 893 cm^{-1}, related to the asymmetric stretching of corner oxygen in W–O–W; νas(W=O) = 983 cm^{-1}, indicative of the asymmetric stretching of the terminal oxygen; and ν(P–O) at 1080 cm^{-1}, assigned to asymmetric stretching of oxygen with a central phosphorous atom) [22, 23]. HPA salts maintain their corner Keggin structure with the addition of different amount of metallic Cs. When $Cs_XH_{3-X}PW_{12}O_{40}$ is supported on Fe-SiO_2, these bands have somewhat changed. The bands at 1080 and 890 cm^{-1} are overlapped by the characteristic band of SiO_2, while these bands at 985 and 794 cm^{-1} shift to 966 and 805 cm^{-1}, respectively.

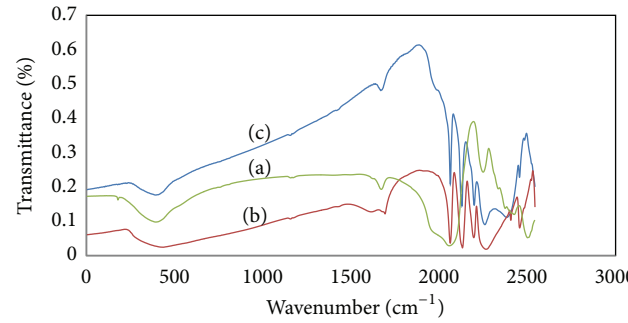

Figure 1: FT-IR spectrums of the $Cs_XH_{3-X}PW_{12}O_{40}$/Fe-SiO_2 (a), $H_3PW_{12}O_{40}$ (b), and $Cs_XH_{3-X}PW_{12}O_{40}$ (c) nanocatalysts.

The XRD pattern of $Cs_XH_{3-X}PW_{12}O_{40}$/Fe-SiO_2 catalyst was presented in Figure 2. Supported HPA samples do not show diffraction patterns probably due to the following reasons: (i) after treatment at 500°C, the HPA practically loses its crystalline structure, (ii) HPA species were highly dispersed, and (iii) the deposited amount of HPA was not big enough to be detected by this technique [24].

The TGA-DSC experiment on the catalyst precursor has shown four steps of mass loss (Figure 3). The first step at the temperature of 70–110°C was attributed to the evaporation of residual moistures in the catalyst precursor and loss of physisorbed waters. The second stage (190–280°C) is accompanying weight loss of the crystallization water expelling

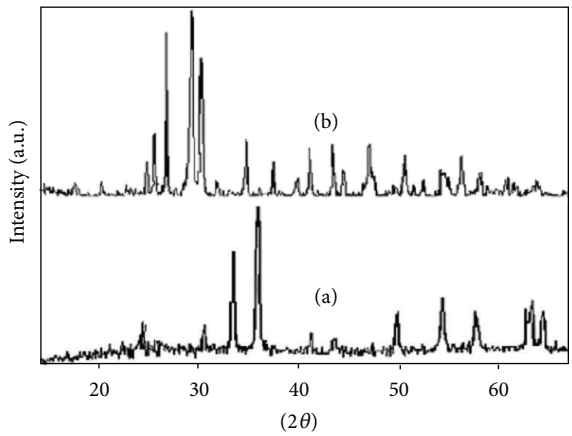

FIGURE 2: XRD patterns of the $Cs_1H_2PW_{12}O_{40}/Fe\text{-}SiO_2$ (a) and $Cs_1H_2PW_{12}O_{40}$ (b) nanocatalysts.

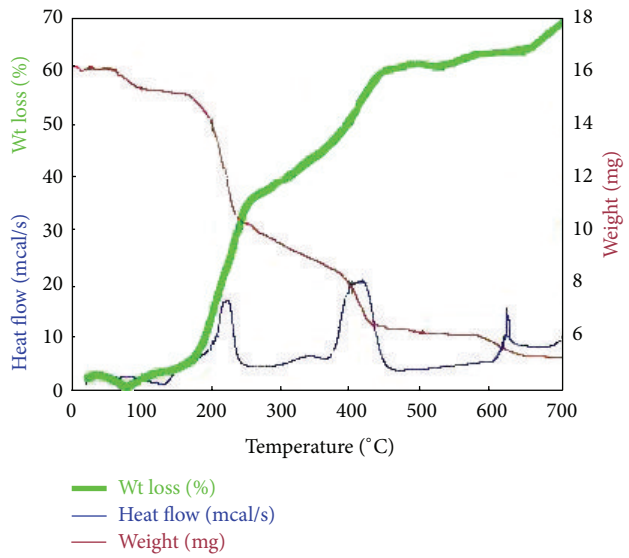

FIGURE 3: TGA and DSC curves for $Cs_XH_{3-X}PW_{12}O_{40}/Fe\text{-}SiO_2$ precursor.

which is most likely the hydrated proton. The peak around 390–460°C is due to the decomposition of iron and Si oxalates to oxide phases. Most of weight loss happened from 580°C to 640°C due to the phase transition and formation of Fe_2SiO_4 (cubic). The weight loss curve is involved with a total overall weight loss of ca. 69 wt%. DSC measurement was performed in order to provide further evidence for the presence of the various species and evaluate their thermal behavior. As shown in Figure 3, the endothermic curve represents the removal of the physically adsorbed water from the material (70–110°C). Two exothermic peaks at around 190–280°C and 390–480°C are due to the crystallization water expelling which is most likely the hydrated proton and the decomposition of iron and Si oxalates to oxide phases, respectively. The exothermic peak at around 580–640°C is due to formation of iron silicate phase [25].

Figure 4 shows SEM pictures of the precursor (a) and calcined catalyst (b). After calcination catalyst particle aggregated together and formed a spherical shape and more uniform particles which are beneficial to the activity and augmenting the surface of the catalyst that exhibited a large amount of aggregates than the precursor. The measured BET surface areas are 237.5 $m^2\ cm^3\ g^{-1}$ for $Cs_XH_{3-X}PW_{12}O_{40}/Fe\text{-}SiO_2$ catalyst and corresponded pore volume is 0.7672 $cm^3\ g^{-1}$ obtained from analysis of the desorption using the BJH (Barrett-Joyner-Halenda) method. The particle size could be calculated by Scherer-equation form XRD pattern (Figure 2). It is clear that the catalyst particle size was in nanodimension (45 nm). The $Cs_XH_{3-X}PW_{12}O_{40}/Fe\text{-}SiO_2$ catalyst was characterized with SEM (Figure 4). It is obvious in this figure that the crystal sizes were from 38–47 nm. This result confirmed the obtained results studied by using the Scherrer equation.

4.2. Calculation of Rate Constant, Activation Energy, and Preexponential Factor. Plots of $-\ln(1 - X_{ME})$ versus (T) are given in Figure 5. Rate constant has been calculated using Figure 5. And activation energy is calculated through the Arrhenius equation:

$$k = Ae^{-E_a/RT} \tag{4}$$

$$\Longrightarrow \ln k = \ln A - \frac{E_a}{RT}, \tag{5}$$

where (k) is the reaction constant, A is the frequency or preexponential factor, E_a is the activation energy of the reaction, R is the gas constant, and T is the absolute temperature.

Therefore, plots of $\ln k$ versus $1/T$ are given in Figure 6. Activation energy (E_a) and preexponential factor have been calculated using Figure 6 to be 79.805 kJ/mol and 8.9×10^8 kJ/mol, respectively. Based on the proposed kinetic model, the kinetic parameters for this catalyst were determined. The experiments demonstrate that the reactions follow first-order kinetics. The proposed kinetic model describes the experimental results well and the rate constants follow the Arrhenius equation.

4.3. Thermodynamic Parameters (ΔS and ΔH). Based on the definition of Gibbs energy free using (7) and using linear plot of $\ln k_{eq}$ versus $\ln 1/T$ which is given in Figure 7 and by using (7) the respective values of ΔS and ΔH were calculated which are 0.0197 kJ/mol, 79.784 kJ/Kmol respectively:

$$\Delta G = -RT \ln k_{eq} \tag{6}$$

$$\ln k_{eq} = \frac{\Delta S}{R} - \frac{\Delta H}{RT}. \tag{7}$$

From the results (Table 2) of the thermodynamic parameters it can be found that the transesterification reaction is an endothermic reaction and, with increasing temperature, reaction rate increases. Moreover, enthalpy and entropy change are not affected by methanol concentration due to its excess [26].

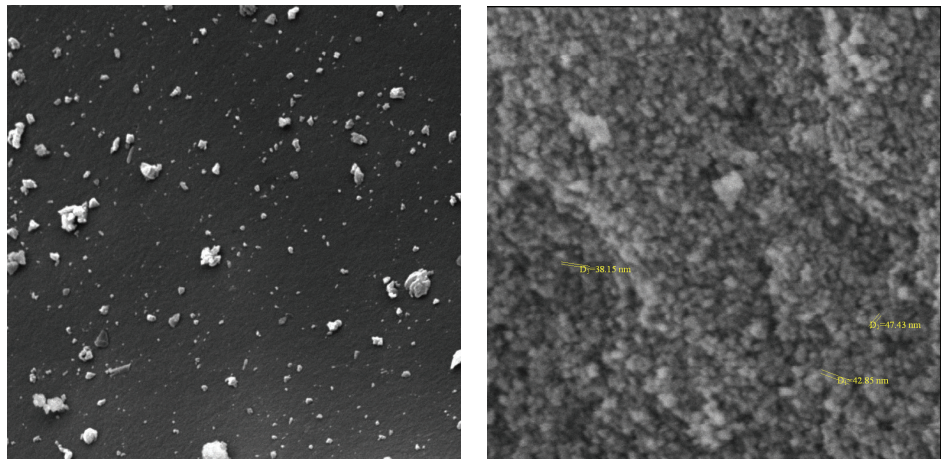

(a) (b)

Figure 4: The SEM images of $Cs_XH_{3-X}PW_{12}O_{40}$/Fe-SiO_2 nanocatalyst, (a) precursor and (b) calcined catalyst.

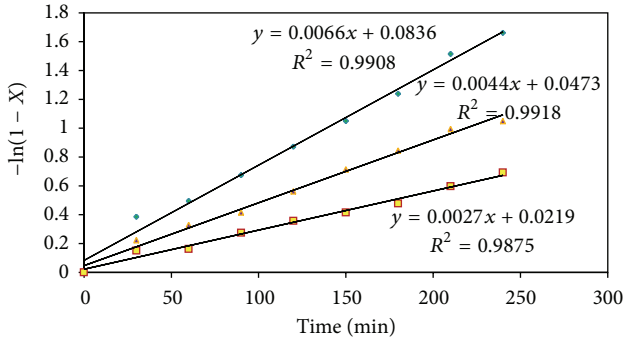

Figure 5: Plots of $-\ln(1-X)$ versus time (min) at temperatures 60, 55, and 50°C for reaction of sunflower oil with methanol.

Table 2: Calculated values of thermodynamic parameters.

T (K)	ΔG (kJ/K·mol)	ΔH (kJ/K·mol)	ΔS (KJ/mol)
323	26.83272		
328	25.98118	79.784	0.0197
333	25.19303		

5. Conclusions

The magnetic $Cs_XH_{3-X}PW_{12}O_{40}$/Fe-SiO_2 nanocatalyst was prepared for biodiesel production. Experimental conditions were varied as follows: reaction temperature 328–338 K, methanol/oil molar ratio = 12/1, and the reaction time 0–240 min. Thermodynamic properties such as ΔS and ΔH were successfully determined from equilibrium constants measured at different temperature. Activation energy (E_a) and preexponential factor have been calculated to be 79.805 kJ/mol and 8.9×10^8 kJ/mol, respectively. The experiments demonstrate that the reactions follow first-order kinetics. Also notably, recovery of the catalyst can be achieved easily with the help of an external magnet in a very short time (<20 seconds) with no need for expensive ultracentrifugation.

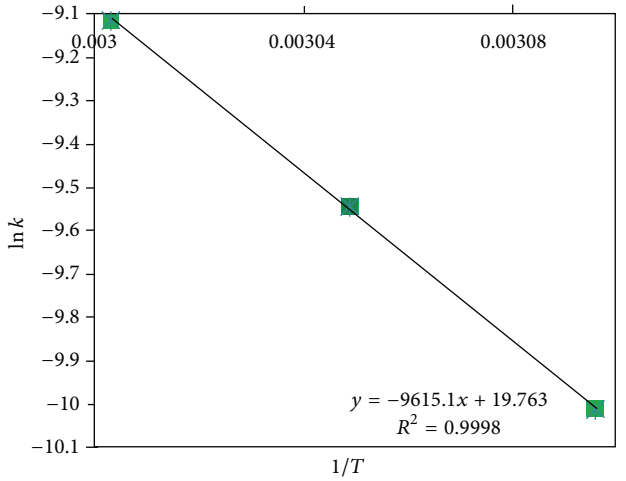

Figure 6: Arrhenius plot of ln k versus $1/T$ for reaction of sunflower oil with methanol.

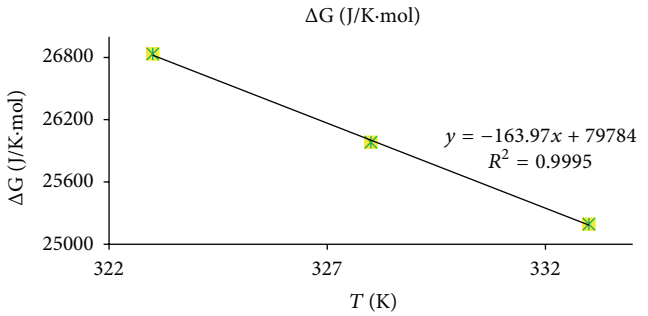

Figure 7: Plot of ΔG (J/K·mol) versus T (K) for reaction of sunflower oil with methanol.

Acknowledgment

The authors are grateful to the Iran Nanotechnology Initiative Council (INIC) for its partial support of this project.

References

[1] M. C. Math, S. P. Kumar, and S. V. Chetty, "Technologies for biodiesel production from used cooking oil: a review," *Energy for Sustainable Development*, vol. 14, no. 4, pp. 339–345, 2010.

[2] P.-L. Boey, G. P. Maniam, and S. A. Hamid, "Performance of calcium oxide as a heterogeneous catalyst in biodiesel production: a review," *Chemical Engineering Journal*, vol. 168, no. 1, pp. 15–22, 2011.

[3] E. H. Pryde, "Vegetable oils as fuel alternatives: symposium overview," *Journal of the American Oil Chemists Society*, vol. 61, no. 10, pp. 1609–1610, 1984.

[4] J. M. Dias, M. C. M. Alvim-Ferraz, and M. F. Almeida, "Comparison of the performance of different homogeneous alkali catalysts during transesterification of waste and virgin oils and evaluation of biodiesel quality," *Fuel*, vol. 87, no. 17-18, pp. 3572–3578, 2008.

[5] Z. Helwani, M. R. Othman, N. Aziz, J. Kim, and W. J. N. Fernando, "Solid heterogeneous catalysts for transesterification of triglycerides with methanol: a review," *Applied Catalysis A*, vol. 363, no. 1-2, pp. 1–10, 2009.

[6] L. C. Meher, D. Vidya Sagar, and S. N. Naik, "Technical aspects of biodiesel production by transesterification: a review," *Renewable and Sustainable Energy Reviews*, vol. 10, no. 3, pp. 248–268, 2006.

[7] F. Qiu, Y. Li, D. Yang, X. Li, and P. Sun, "The use of heterogeneous catalysts to replace homogeneous ones can be expected to eliminate the problems associated with homogeneous catalysts," *Bioresource Technology*, vol. 102, pp. 4150–4156, 2011.

[8] K. Jacobson, R. Gopinath, L. C. Meher, and A. K. Dalai, "Solid acid catalyzed biodiesel production from waste cooking oil," *Applied Catalysis B*, vol. 85, no. 1-2, pp. 86–91, 2008.

[9] M. Zabeti, W. M. A. Wan Daud, and M. K. Aroua, "Activity of solid catalysts for biodiesel production: a review," *Fuel Processing Technology*, vol. 90, no. 6, pp. 770–777, 2009.

[10] S. Shanmugam, B. Viswanathan, and T. K. Varadarajan, "Esterification by solid acid catalysts: a comparison," *Journal of Molecular Catalysis A*, vol. 223, no. 1-2, pp. 143–147, 2004.

[11] Y. Liu, E. Lotero, and J. G. Goodwin Jr., "A comparison of the esterification of acetic acid with methanol using heterogeneous versus homogeneous acid catalysis," *Journal of Catalysis*, vol. 242, no. 2, pp. 278–286, 2006.

[12] Z. Helwani, M. R. Othman, N. Aziz, W. J. N. Fernando, and J. Kim, "Technologies for production of biodiesel focusing on green catalytic techniques: a review," *Fuel Processing Technology*, vol. 90, no. 12, pp. 1502–1514, 2009.

[13] H.-J. Kim, Y.-G. Shul, and H. Han, "Synthesis of heteropolyacid $(H_3PW_{12}O_{40})/SiO_2$ nanoparticles and their catalytic properties," *Applied Catalysis A*, vol. 299, no. 1-2, pp. 46–51, 2006.

[14] N. Mizuno and M. Misono, "Pore structure and surface area of Cs (x = 0–3, M = W, Mo)," *Chemistry Letters*, vol. 16, pp. 967–970, 1987.

[15] T. Okuhara, T. Ichiki, K. Y. Lee, and M. Misono, "Dehydration mechanism of ethanol in the pseudoliquid phase of $H_{3-X}Cs_XPW_{12}O_{40}$," *Journal of Molecular Catalysis A*, vol. 55, pp. 293–301, 1989.

[16] L. R. Pizzio, P. G. Vázquez, C. V. Cáceres et al., "C-alkylation reactions catalyzed by silica-supported Keggin heteropolyacids," *Applied Catalysis A*, vol. 287, no. 1, pp. 1–8, 2005.

[17] H.-J. Kim, Y.-G. Shul, and H. Han, "Synthesis of heteropolyacid $(H_3PW_{12}O_{40})/SiO_2$ nanoparticles and their catalytic properties," *Applied Catalysis A*, vol. 299, no. 1-2, pp. 46–51, 2006.

[18] X. Zhao, Y. Han, X. Sun, and Y. Wang, "Structure and catalytic performance of $H_3PW_{12}O_{40}/SiO_2$ prepared by several methods," *Chinese Journal of Catalysis*, vol. 28, no. 1, pp. 91–96, 2007.

[19] Q. Shu, J. Gao, Y. Liao, and J. Wang, "Reaction kinetics of biodiesel synthesis from waste oil using a carbon-based solid acid catalyst," *Chinese Journal of Chemical Engineering*, vol. 19, no. 1, pp. 163–168, 2011.

[20] S. Saka and D. Kusdiana, "Biodiesel fuel from rapeseed oil as prepared in supercritical methanol," *Fuel*, vol. 80, no. 2, pp. 225–231, 1998.

[21] D. Kusdiana and S. Saka, "Kinetics of transesterification in rapeseed oil to biodiesel fuel as treated in supercritical methanol," *Fuel*, vol. 80, no. 5, pp. 693–698, 2001.

[22] K. Srilatha, R. Sree, B. L. A. Prabhavathi Devi, P. S. S. Prasad, R. B. N. Prasad, and N. Lingaiah, "Preparation of biodiesel from rice bran fatty acids catalyzed by heterogeneous cesium-exchanged 12-tungstophosphoric acids," *Bioresource Technology*, vol. 116, pp. 55–57, 2012.

[23] L. Nakka, J. E. Molinari, and I. E. Wachs, "Surface and bulk aspects of mixed oxide catalytic nanoparticles: oxidation and dehydration of CH_3OH by polyoxometallates," *Journal of the American Chemical Society*, vol. 131, no. 42, pp. 15544–15554, 2009.

[24] J. C. Yori, J. M. Grau, V. M. Benítez, and J. Sepúlveda, "Hydroisomerization-cracking of n-octane on heteropolyacid $H_3PW_{12}O_{40}$ supported on ZrO_2, SiO_2 and carbon Effect of Pt incorporation on catalyst performance," *Applied Catalysis A*, vol. 286, no. 1, pp. 71–78, 2005.

[25] Q. Deng, W. Zhou, X. Li et al., "Microwave radiation solid-phase synthesis of phosphotungstate nanoparticle catalysts and photocatalytic degradation of formaldehyde," *Journal of Molecular Catalysis A*, vol. 262, no. 1-2, pp. 149–155, 2007.

[26] S. A. Fernandes, A. L. Cardoso, and M. J. Da Silva, "A novel kinetic study of $H_3PW_{12}O_{40}$: catalyzed oleic acid esterification with methanol via HNMR spectroscopy," *Fuel Processing Technology*, vol. 96, pp. 98–103, 2012.

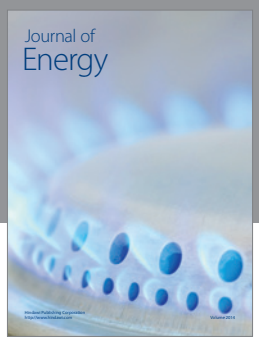

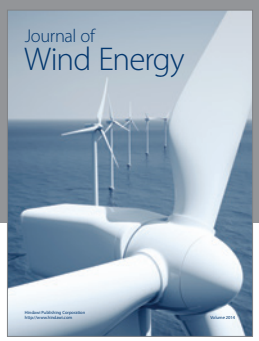

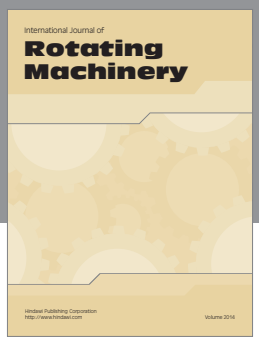

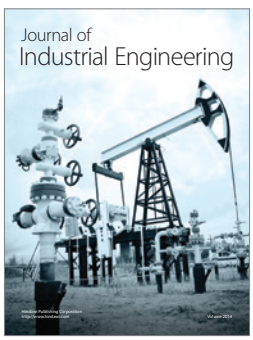

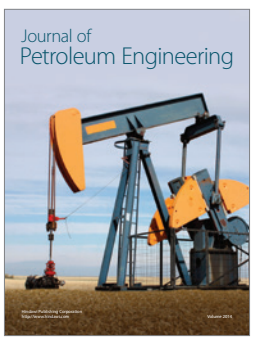

Hindawi
Submit your manuscripts at
http://www.hindawi.com